Pharm Res (2014) 31:278–290
DOI 10.1007/s11095-013-1159-4

RESEARCH PAPER

Radioiodinated Hypericin: Its Biodistribution, Necrosis Avidity and Therapeutic Efficacy are Influenced by Formulation

Marlein Miranda Cona • Yeranddy Aguiar Alpizar • Junjie Li • Matthias Bauwens • Yuanbo Feng • Ziping Sun • Jian Zhang • Feng Chen • Karel Talavera • Peter de Witte • Alfons Verbruggen • Raymond Oyen • Yicheng Ni

Received: 3 February 2013 / Accepted: 22 July 2013 / Published online: 9 August 2013

ABSTRACT

Purpose To study whether formulation influences biodistribution, necrosis avidity and tumoricidal effects of the radioiodinated hypericin, a necrosis avid agent for a dual-targeting anticancer radiotherapy.

Methods Iodine-123- and 131-labeled hypericin (^{123}I-Hyp and ^{131}I-Hyp) were prepared with Iodogen as oxidant, and formulated in dimethyl sulfoxide (DMSO)/PEG400 (polyethylene glycol 400)/water (25/60/15, v/v/v) or DMSO/saline (20:80, v/v). The formulations with excessive Hyp were optically characterized. Biodistribution, necrosis avidity and tumoricidal effects were studied in rats ($n = 42$) without and with reperfused liver infarction and implanted rhabdomyosarcomas (R1). To induce tumor necrosis, R1-rats were pre-treated with a vascular disrupting agent. Magnetic resonance imaging, tissue-gamma counting, autoradiography and histology were used.

Results The two formulations differed significantly in fluorescence and precipitation. ^{123}I-Hyp/Hyp in DMSO/PEG400/water exhibited high uptake in necrosis but lower concentration in the lung, spleen and liver ($p < 0.01$). Tumor volumes of 0.9 ± 0.3 cm^3 with high radioactivity (3.1 ± 0.3% ID/g) were detected 6 days post-treatment. By contrast, ^{131}I-Hyp/Hypin DMSO/saline showed low uptake in necrosis but high retention in the spleen and liver ($p < 0.01$). Tumor volumes reached 2.6 ± 0.7 cm^3 with low tracer accumulation (0.1 ± 0.04%ID/g).

Conclusions The formulation of radioiodinated hypericin/hypericin appears crucial for its physical property, biodistribution, necrosis avidity and tumoricidal effects.

KEY WORDS cancer · formulation · OncoCiDia · radioiodinated hypericin · targeted radiotherapy

ABBREVIATIONS

^{123}I-Hyp	Iodine-123-labeled hypericin
^{131}I-Hyp	Iodine-131-labeled hypericin
%ID	Percentage of injected dose
%ID/g	Percentage of injected dose per gram of tissue

Electronic supplementary material The online version of this article (doi:10.1007/s11095-013-1159-4) contains supplementary material, which is available to authorized users.

M. M. Cona • J. Li • Y. Feng • F. Chen • R. Oyen • Y. Ni
Department of Imaging & Pathology, Faculty of Medicine
Biomedical Sciences Group KU Leuven
Herestraat 49, Leuven, Belgium

M. M. Cona • J. Li • Y. Feng • F. Chen • Y. Ni
Molecular Small Animal Imaging Centre/MoSAIC, Faculty of Medicine
Biomedical Sciences Group
KU Leuven Herestraat 49, Leuven, Belgium

Y. A. Alpizar • K. Talavera
Laboratory of Ion Channel Research
Department of Cellular and Molecular Medicine
KU Leuven Herestraat 49, Leuven, Belgium

M. Bauwens • P. de Witte • A. Verbruggen
Faculty of Pharmaceutical Sciences, Biomedical Sciences Group KU Leuven Herestraat 49, Leuven, Belgium

Z. Sun • Y. Ni
Radiopharmacy Laboratory, Shandong Academy of Medical Sciences
Jinan 250062, China

J. Zhang • Y. Ni
Laboratory of Translational Medicine
Jiangsu Academy of Traditional Chinese Medicine
Nanjing 210028, China

Y. Ni (✉)
Theragnostic Laboratory, Radiology KU Leuven UZ Gathuisberg
Herestraat 49, 3000 Leuven, Belgium
e-mail: Yicheng.Ni@med.kuleuven.be

AutoRx	Autoradiography
CE-MRI	Contrast enhanced -magnetic resonance imaging
DLU	Digital light units
DMSO	Dimethyl sulfoxide
Gd-DOTA	Gadolinium-tetraazacyclododecanetetraacetic acid
H&E	Hematoxylin and eosin
HA	Histological analysis
HPLC	High performance liquid chromatography
Hyp	1,3,4,6,8,13-Hexahydroxy-10, 11-dimethylphenanthro[1,10,9,8-opqra]perylene-7, 14-dione or Hypericin
Iodogen	1,3,4,6-tetrachloro-3alpha,6alpha-diphenylglycouril
IV	Intravenous
M	Macroscopy
MPS	Mononuclear phagocyte system
NR	Necrosis ratio
OM	Optical microscopy
PBS	Phosphate buffered saline
PEG400	Polyethylene glycol 400
R1	Rhabdomyosarcoma tumors
RES	Reticuloendothelial system
ROI	Regions of interest
RPLI	Reperfused partial liver infarction
SD	Standard deviation
TGC	Tissue gamma counting
TV	Tumor volume
VDA	Vascular disrupting agent
ZD6126	N-Acetylcolchicinol dihydrogenphosphate

INTRODUCTION

Cancer treatment is challenging. Surgery, external beam radiotherapy and chemotherapy are conventionally used to treat the disease or to inhibit tumor growth. However, in patients with disseminated or resistant cancers, implementation of effective targeted therapies is deemed mandatory. Among many others, OncoCiDia has emerged as an unconventional anticancer strategy aiming at improved cancer treatability with a unique soil-to-seeds principle (1,2).

Rather than directly attacking cancer cells that are characterized with escape mechanisms (3), the dual-targeting OncoCiDia hits two stable intratumoral targets that are not cancer cells but closely related to them in functionality and location. The initial administration of a vascular disrupting agent (VDA) selectively occludes tumor blood vessels with immature endothelium and causes ischemic necrosis, which though always leaves a peripheral viable rim as culprit for tumor recurrence (4). To tackle this, iodine-131-labeled hypericin is intravenously given, which preferentially localizes at the newly-formed necrotic core. From there, it kills residual cancer cells through the cross-fire effect of beta radiation (1). The concurrent gamma rays facilitate scintigraphy for improved tumor detectability (2). Promising theragnostic anticancer effects and favorable safety profiles have been demonstrated in rodents without and with different tumor engrafts (2,5–7).

Iodine-123 or iodine-131-labeled hypericin (^{123}I-Hyp or ^{131}I-Hyp) is a radioiodinated derivative of Hypericin (Hyp), a naturally occurring pigment derived from the plant St. John's wort, which has newly been found with a potent *in vivo* necrosis avidity (8,9), in addition to its many other known utilities (10,11). Radioiodinated Hyp is obtained *via* electrophilic substitution by incorporating an oxidized radioactive iodine atom into the aromatic structure of Hyp (Fig. 1) (5,12–14).

Hyp is a highly lipophilic molecule. It dissolves monomolecularly up to concentrations of $2–5 \times 10^{-2}$ mol/l (15) in polar solvents such as dimethyl sulfoxide (DMSO) (16,17), ethanol (18,19) and polyethylene glycol 400 (PEG400) (20,21), and in biological media (22); producing red and highly fluorescent solutions. Unfortunately, Hyp shows poor solubility in neutral pH water-based formulations (10^{-3} mol/l) (23), which otherwise should be more biocompatible and mostly used for parenteral administration in humans. Under aqueous environment, Hyp forms monobasic salts (24,25) that behave as lipophilic ion pairs and are poorly soluble at the pH range of 4–11, leading to non-fluorescent colloidal aggregates (26). Upon systemic administration, instead of targeting to necrosis, the formed aggregates are retained by organs of mononuclear phagocyte system (MPS) or reticuloendothelial system (RES) with phagocytic capacity (27).

Unlike conventional drug chemistry, radiopharmaceutical chemistry uses very small amounts of reagents and isotopes. These small quantities of mass usually emit sufficient radiations to produce desired diagnostic or therapeutic effects. As such, the solubility concerns are usually negligible. However, for the OncoCiDia, the best results so far have been achieved by using a mixture of radioiodinated Hyp/unlabeled Hyp in a concentration range near or below 10^{-3} mol/l, in which hypericin may start to precipitate in aqueous solutions. Moreover, since the incorporation of halogen atoms into a molecule often results in derivatives that are more lipophilic and less water soluble (28,29). Thus, similar to Hyp, a wrong formulation of ^{123}I-Hyp or ^{131}I-Hyp mixed with unlabeled Hyp could cause high uptake in RES organs, leading to an increased irradiation burden in the body along with a poor targeting to necrosis. Subsequently, manifestation of treatment-related adverse effects due to irradiation overexposure of normal tissues in addition to inefficient lethal radiation dose into the necrotic tumors may occur.

Therefore, we hypothesized that the radioiodinated Hyp could retain the lipophilicity and water insolubility of Hyp that might boost the formation of radioactive aggregates in aqueous conditions. To test this hypothesis, we performed *in vivo* studies to investigate and compare different formulations of

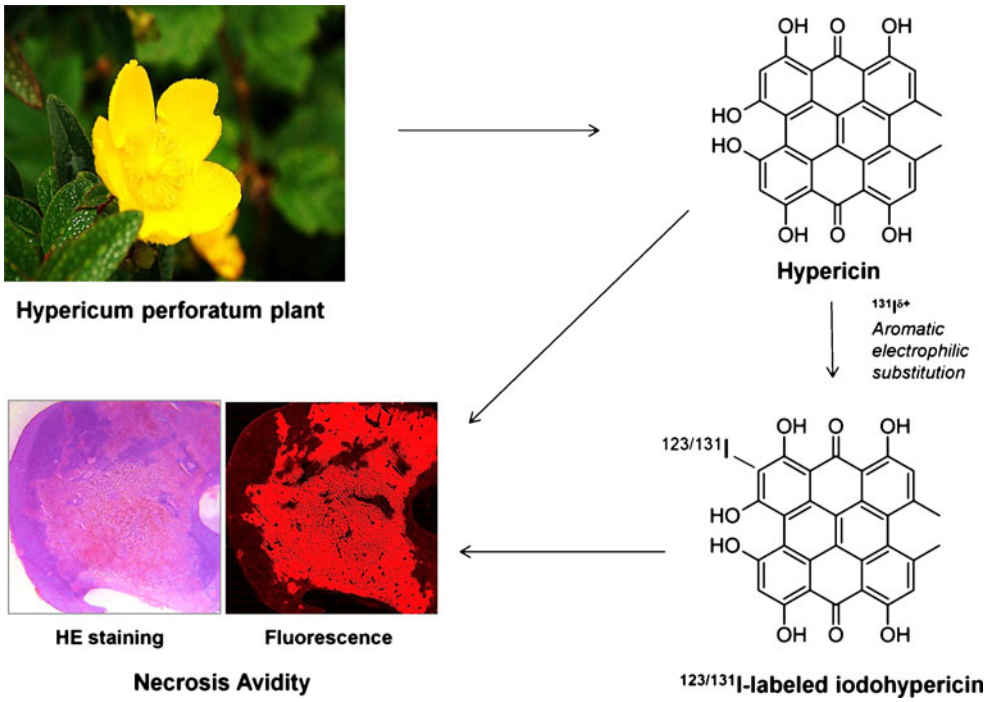

Fig. 1 Schematic representation of hypericin, a naphtodiantrone extracted from Hypericum perforatum plant, and iodine-123/iodine-131-labeled iodohypericin obtained by iodine-123/131 incorporation into hypericin rings *via* aromatic electrophilic substitution. Both compounds are found with strong and long-lasting affinity for necrotic tissues as proven by fluorescent and light microscopy (× 4).

^{123}I-Hyp/Hyp or ^{131}I-Hyp/Hyp for their properties of aggregate sequestration in undesired organs, necrosis avidity and tumoricidal effects.

Our study indicated that because the exact formulation may impact on the pharmacokinetic profile and therapeutic effect of radioiodinated Hyp, a proper delivery system is needed to minimize the aggregate formation before and by systemic administration. It should guarantee efficient transfer of radioiodinated hypericin to serum lipoproteins (30), high accumulation and prolonged retention in necrosis, and subsequently, sufficient cumulative radiation dose on cancer cells. Therefore, further optimizations are needed before OncoCiDia can be applied in clinic.

MATERIALS AND METHODS

Involved Drugs and Chemicals

Hypericin, 1,3,4,6,8,13-Hexahydroxy-10,11-dimethyl-phenanthro[1,10,9,8-opqra]perylene-7,14-dione (Hyp), with a purity greater than 98% was purchased from Planta Natural Products (Austria; http://www.planta.at/hyper/hyper.htm).

The vascular-disrupting agent, N-Acetylcolchicinol dihydrogenphosphate (ZD6126) was acquired from AstraZeneca (Cheshire, UK). All other used chemicals and solvents were reagent grade and received from commercial sources.

Radiolabelling

Radioiodination of Hyp with ^{123}I-sodium iodide (^{123}I-NaI) (901 mCi/ml; GE Healthcare, Diegem, Belgium) or ^{131}I-sodium iodide (^{131}I-NaI) (>500 mCi/ml; Perkin Elmer Life and Analytical Sciences, Boston, MA, USA) was performed using 1,3,4,6-tetrachloro-3alpha,6alpha-diphenylglycouril (Iodogen) (Sigma Chemical Co., St Louis, USA) as oxidizing agent in 90/10% (v/v) DMSO/0.5 M sodium phosphate buffer, at pH 7.4 and room temperature for 30 min (12). The final product consisted of a mixture of radioiodinated Hyp ($\sim 1 \times 10^{-9}$ mol) and unlabeled Hyp ($\sim 1.9 \times 10^{-6}$ mol).

For studies on distribution in RES organs and necrosis avidity, Hyp was labeled with the gamma emitter iodine-123 with a short half-life of 13.2 h. Because iodine-131 emits beta radiation and has a longer half-life of 8.1 days, ^{131}I-Hyp/Hyp was prepared to evaluate affinity for tumor necrosis and tumoricidal effect.

HPLC Analysis

Determination of radiochemical yield was conducted on a high performance liquid chromatography (HPLC) system (LaChrom Elite, Hitachi, Darmstadt, Germany) equipped with a XTerra® C18 analytical column, 5 µm, 4.6 mm × 150-mm (Waters Corporation, Milford, MA, USA), a UV absorbance (254 nm) and a flow-through radioactivity detectors. Sample injection was carried out through a Rheodyne injector valve and then eluted with acetonitrile/0.05 M ammonium

acetate buffer pH 7.0 in gradient mode; at a flow rate of 1.0 ml/min. Acquisition, integration and evaluation of the output signals were done using GinaStar acquisition software (version 4.4; Raytest, Straubenhardt, Germany).

Formulation and Characterization

The radioiodinated hypericin/unlabeled hypericin (^{123}I-Hyp/Hyp or ^{131}I-Hyp/Hyp) (~1.0×10^{-7} mol/l/~2.0×10^{-4} mol/l) was prepared in two formulations of either DMSO/saline (20:80, v/v) or DMSO/PEG400/water (25:60:15, v/v/v). For evaluation on physical properties of the solution, each formulation was macroscopically inspected and digitally photographed (Canon Digital IXUS 860 IS). For assessment of fluorescent properties, digital images were shot in a CN-15 darkroom cabinet (Vilber Lourmat Deutschland GmbH) at 254 nm as excitation wavelength. Numerous other formulations were also screened *in vitro* (see Supplementary Materials).

To evaluate aggregate formation, microscopic observations over a drop (1.0 µl) of ^{123}I-Hyp/Hyp or ^{131}I-Hyp/Hyp dissolved in DMSO/PEG400/water (25:60:15, v/v/v) or DMSO/saline (20:80, v/v) were performed by using a MT–10 illumination system (Olympus, Planegg, Germany). Images were acquired either in bright field or fluorescence illumination mode at 50 µm × magnifications. Cross-sectional fluorescence intensity profiles (absorbance unit) along red-continuing lines (n=5) over the drop (µm) were generated using a Cell^M software (Olympus, Planegg, Germany) at an exposure time of 20 ms and 1×1 binning factor.

Experimental Design

All experimental procedures were approved by the local Animal Ethics Committee and were according to European Ethics Committee guidelines (decree 86/609/EEC). As illustrated in Fig. 2, a total of 42 adult male WAG/Rij rats weighing 300–350 g were used for the experiments. The animals were purchased from Charles River Breeding Laboratories, Inc. (St. Aubain les Elbeuf, France).

Distribution of ^{123}I- Hyp/Hyp in RES Organs

Biodistribution of ^{123}I-Hyp/Hyp in different formulations in RES organs was evaluated in 12 normal rats. The animals (n=6/formulation) were intravenously (IV) injected with a dose of 12.0 MBq/400 µl of ^{123}I-Hyp/Hyp in DMSO/PEG400/water (25:60:15, v/v/v) or DMSO/saline (20:80, v/v), under intraperitoneal anesthesia with 30 mg/kg pentobarbital sodium (Nembutal) (Sanofi Sante Animale, Brussels, Belgium). The rats were killed by an overdose of Nembutal 24 h later.

After animal dissection, the liver, spleen, and lungs were weighed and radioactivities were counted for 1 min (cpm) using a gamma counter (3-in NaI(Tl)) well crystal coupled to a multichannel analyzer (Wallac 1480 Wizard 3″, Wallac, Turku, Finland). The rest of body, urine and feces were also collected and their radioactive contents were measured for determination of the total injected dose. Radioactivity concentrations were expressed as percentage of injected dose (%ID) and percentage of injected dose per gram of tissue (%ID/g).

Necrosis Avidity of ^{123}I- Hyp/Hyp

Uptake of ^{123}I-Hyp/Hyp in liver necrosis was assessed in 12 rats of reperfused partial liver infarction (RPLI) in the right liver lobe, as previously described (31,32).

One day after RPLI, the rats (n=6/formulation) were anesthetized with intraperitoneal Nembutal (30 mg/kg) and IV injected with a dose of 12.0 MBq/400 µl of ^{123}I-Hyp/Hyp in DMSO/PEG400/water (25:60:15, v/v/v) or DMSO/saline (20:80, v/v). The animals were then sacrificed with overdosed

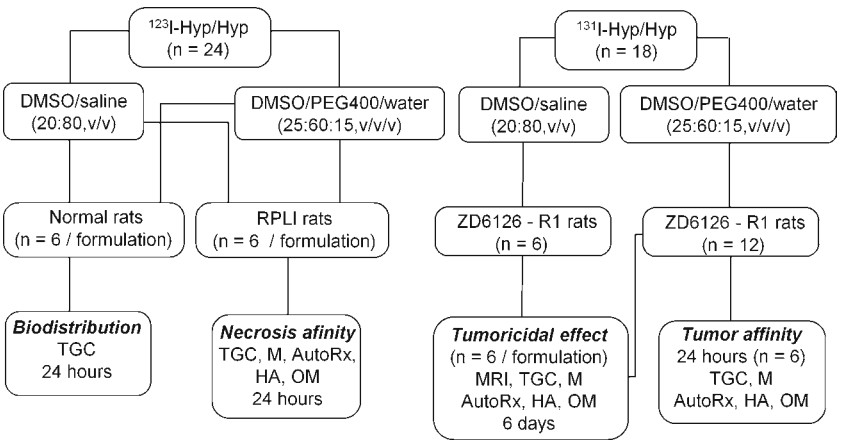

Fig. 2 Flow diagram of the experimental procedures. AutoRx: autoradiography, DMSO: dimethyl sulfoxide, M: Microscopy, HA: histological analysis, ^{123}I-Hyp/Hyp: Iodine-123-labeled hypericin/hypericin, ^{131}I-Hyp/Hyp: Iodine-131-labeled hypericin/hypericin, OM: optical microscopy, PEG: polyethylene glycol, R1: rhabdomyosarcoma (R1) tumors, RPLI: reperfused partial liver infarction, TGC: tissue gamma counting, ZD6126: N-Acetylcolchicinol dihydrogenphosphate.

Nembutal after 24 h. The necrotic and viable liver lobes were dissected, weighed and their radioactivities were counted. The rest of the body, urine and feces were also measured for radioactive counts to calculate the total injected dose. Radioactivity uptakes in necrotic and viable liver lobes were expressed as %ID, %ID/g and mean %ID/g ratios between necrotic and viable tissues.

Samples of necrotic and viable liver from RPLI rats were frozen in dry ice cooled isopentane. The freezing tissues were cut with a cryotome (Shandon Cryotome FSE; Thermo Fisher, Waltham, USA) into 50- and 10-μm sections, which were thaw-mounted on glass slides. Autoradiographs were performed by exposing the sections to a super resolution screen (Canberra-Packard, Meridan, USA) for 48 h. Digital autoradiographic images were obtained by reading out the phosphor screen using a Cyclone Phosphor Imager scanner (Canberra-Packard, Meridan, USA). Regions of interest (ROI) from the images were analyzed with Optiquant software (version 5.0; Canberra-Packard, Meridan, USA). Activity concentration was expressed in digital light units (DLU)/mm^2. Ratios of activity concentration (DLU/mm^2) between ROIs on necrotic and viable areas were calculated.

The 50- and 10-μm sections were stained with hematoxylin and eosin (H&E). The 50-μm sections were digitally photographed for macroscopic inspection. The 10-μm sections were microscopically examined (Zeiss Axiophot Microscope; Oberkochen, Germany).

Avidity of ^{131}I-Hyp/Hyp for Tumor Necrosis

Avidity for tumor necrosis of ^{131}I-Hyp/Hyp was evaluated in 6 rats with rhabdomyosarcomas (R1) implanted in the liver using a reported technique (33).

After gas anesthesia using 2% isoflurane (Halocarbon, River Edge, NJ, USA) mixed with 20% of O2 and 80% of air, a VDA ZD6126 was IV injected at a dose of 20 mg/kg to induce tumor necrosis. Before and 24 h after VDA administration, T1-weighted magnetic resonance imaging (MRI) with gadolinium-tetraazacyclododecanetetraacetic acid (Gd-DOTA, Dotarem, Guerbet, France) enhancement was performed at 0.1 mmol/kg using a 1.5 T scanner (Sonata, Siemens, Erlangen, Germany) to determine tumor vascular shutdown and necrosis.

The day prior to ZD6126 administration, the R1 rats received 18.0 MBq/600 μl of ^{131}I-Hyp/Hyp in DMSO/PEG400/water (25:60:15, v/v/v). Animals were sacrificed 24 h later, and liver and tumor samples were harvested, weighted and counted. The rest of the body, feces and urine were also collected for determining the total injected dose of radioactivity. Tumor samples were analyzed by autoradiography and H&E stained histology. Tumor and normal liver uptake of ^{131}I-Hyp/Hyp were expressed as %ID/g and radioactivity uptake ratios between tumor necrosis and viable liver by radioactivity counting and autoradiography.

Tumoricidal Effects of ^{131}I-Hyp/Hyp

Assessment of therapeutic effects of ^{131}I-Hyp/Hyp in DMSO/PEG400/water (25:60:15, v/v/v) or DMSO/saline (20:80, v/v) was conducted on 12 rats with R1 implanted in the liver. The rats were housed in separate cages in environmentally controlled rooms (19–20°C) under a 14 h light and 10 h dark cycle. Food (Ssniff Spezialdiäten GmbH, Soest, Germany) and water were given *ad libitum*.

On the day prior to the radioactivity administration, tumor necrosis was induced by ZD6126 at an IV dose of 20 mg/kg. The animals were then injected with 111 MBq/600 μl of ^{131}I-Hyp/Hyp in DMSO/PEG400/water (25:60:15, v/v/v) or DMSO/saline (20:80, v/v) after 24 h. CE-MRI was acquired before and serially till 7 days after ZD6126 injection to monitor the tumor vascular shutdown and tumoricidal effects. Tumor volume and tumor necrosis ratio (%) at 24 h and 6 days after radioactivity administration were determined by CE-MRI.

After *in vivo* studies, R1 rats were killed by overdosed Nembutal and dissected. Tumors were harvested, weighed and examined macroscopically, and further counted for %ID/g and analyzed by autoradiography and H&E histology. Urine, feces and rest of the body were also collected for determination of the total injected radiation dose.

Statistical Analysis

Quantitative data were expressed as mean ± SD. Statistical analysis was carried out using GraphPad Prism (version 4.0; Graph Pad, San Diego, USA) by a paired Student's *t*-test. P value <0.05 or <0.01 was considered statistically significant.

RESULTS

Radiolabelling and HPLC Analysis

Hyp was efficiently radioiodinated by using Iodogen as oxidizing agent (5,12). A mixture of radioiodinated Hyp ($\sim 1\times10^{-9}$ mol) and starting unlabeled Hyp ($\sim 1.9\times10^{-6}$ mol) was obtained. Figure 3 shows a typical HPLC chromatogram with UV absorbance and radiochemical detection. From HPLC analysis, ^{123}I-Hyp and ^{131}I-Hyp were efficiently prepared with a radiochemical yield around 95.0% and specific activity above 90 MBq/μmol. On radio-HPLC chromatogram, a main, sharp peak corresponding to ^{123}I-Hyp or ^{131}I-Hyp appeared with a retention time (RT) of 11.57 min. A second, small peak with a RT of 12.31 min corresponded to di-iodinated hypericin, as was confirmed using mass spectrometry (MS) analysis. By UV absorbance, at 1.49 min of RT, a peak was observed corresponding to the reaction solvent DMSO. The broad peak of unlabeled Hyp appeared later with a RT of 7.85 min.

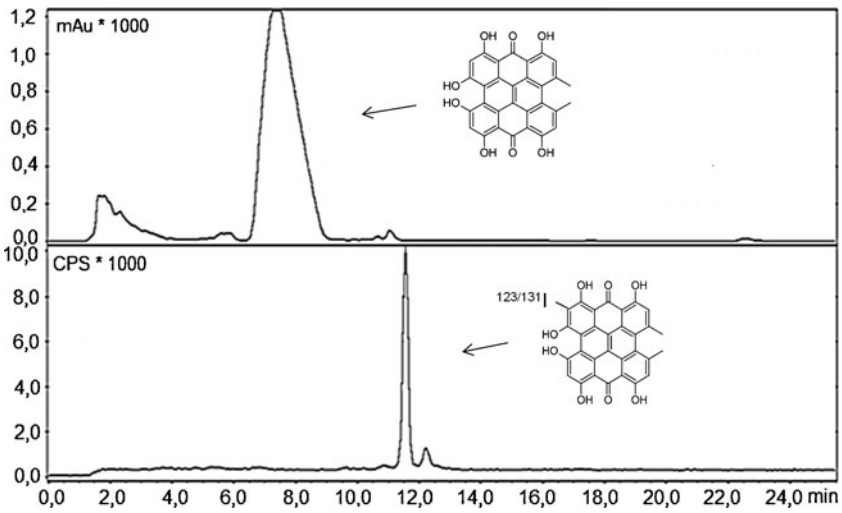

Fig. 3 HPLC UV-chromatogram of unlabeled hypericin (Hyp) with a retention time of 7.85 min (*upper part*) and HPLC radiochromatogram (*lower part*) of iodine-123/iodine-131-labeled hypericin ($^{123/131}$I-Hyp) with a retention time of 11.57 min.

Formulations and Optical Characterization

The radioactive compounds ^{123}I-Hyp/Hyp and ^{131}I-Hyp/Hyp were prepared in two different formulations, i.e. DMSO/PEG400/water (25:60:15, v/v/v) and DMSO/saline (20:80, v/v). When ^{123}I-Hyp/Hyp or ^{131}I-Hyp/Hyp was in DMSO/PEG400/water (25:60:15, v/v/v), it formed a clear reddish "true" solution with strong fluorescence, as

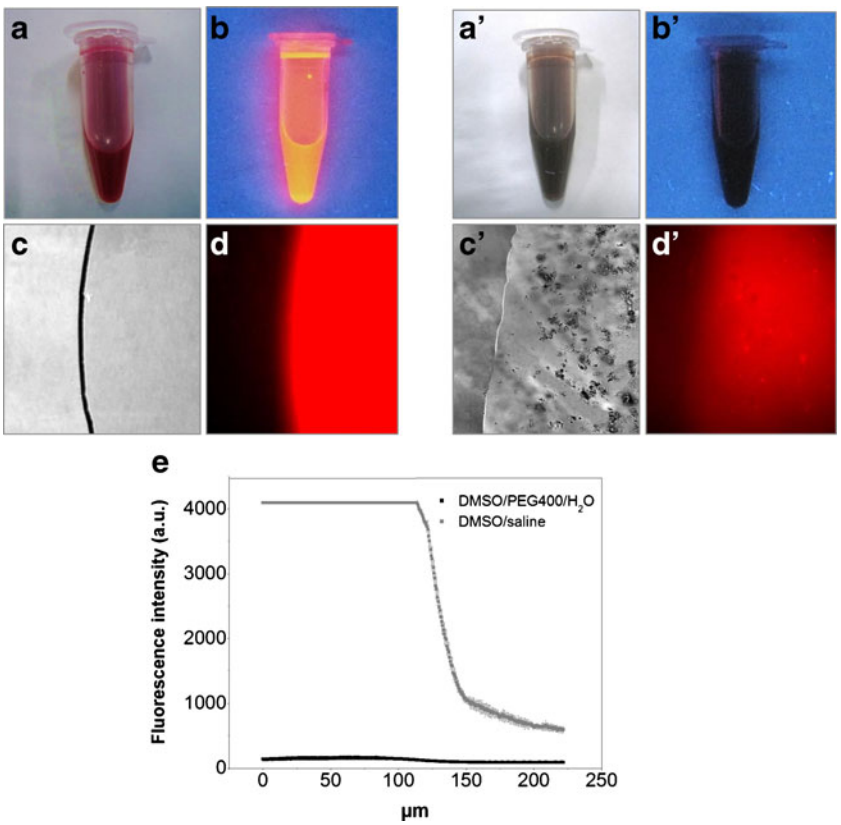

Fig. 4 Characterization of different formulations of radioiodinated Hyp/Hyp (~1.0×10^{-7} mol/l/~2.0×10^{-4} mol/l). ^{123}I-Hyp/Hyp or ^{131}I-Hyp/Hyp in DMSO/PEG400/water (25:60:15, v/v/v) showed as a clear red solution (**a**) with strong fluorescence at 254 nm (**b**). Microscopic views on a drop of ^{123}I-Hyp/Hyp or ^{131}I-Hyp/Hyp in this formulation demonstrated a clean field without aggregates formation under bright field mode (**c**) and intense homogenous fluorescence (**d**). By contrast, ^{123}I-Hyp/Hyp or ^{131}I-Hyp/Hyp in DMSO/saline (20:80, v/v) formed a cloudy brownish solution (**a'**) without fluorescence (**b'**). By microscopy, formation of aggregates (**c'**) and reduced fluorescent intensity (**d'**) were observed. Cross-sectional fluorescence intensity profiles over a drop of each formulation are distinguished for a high homogeneous fluorescence from ^{123}I-Hyp/Hyp or ^{131}I-Hyp/Hyp in DMSO/PEG400/water (25:60:15, v/v/v) in contrast with a twenty-fold lower fluorescence in DMSO/saline (20:80, v/v) formulation (**e**).

viewed under tungsten light or at 254 nm respectively (Fig. 4). Microscopically, ^{123}I-Hyp/Hyp or ^{131}I-Hyp/Hyp in DMSO/PEG400/water (25:60:15, v/v/v) looked clean without discernible aggregates under bright illumination and highly fluorescent under green excitation light (519 nm) as proven by a high profile of homogeneous fluorescence (Fig. 4). By contrast, ^{123}I-Hyp/Hyp or ^{131}I-Hyp/Hyp in DMSO/saline (20:80, v/v) appeared as a cloudy brownish solution without fluorescent emission (Fig. 4). Microscopy confirmed aggregate formation and colloidal feature of ^{123}I-Hyp/Hyp or ^{131}I-Hyp/Hyp with reduced fluorescent properties. Cross-sectional fluorescence intensity profiles showed a twenty-fold lower fluorescence than that of DMSO/PEG400/water-based formulation (Fig. 4).

Results on the physical properties of other 12 formulations of radioiodinated Hyp/Hyp evaluated by using macroscopic and microscopic techniques are shown in the Supplementary Materials.

Animal Studies

All animals survived the anesthesia, surgery, tumor development and *in vivo* imaging. RPLI and R1 tumor models were successfully established. In rats with R1, no spontaneous necrosis but massive intratumoral necrosis were observed before and 24 h after administration of ZD6126, as evidenced by *in vivo* CE-MRI.

Distribution of ^{123}I- Hyp/Hyp in RES Organs

The biodistributions of ^{123}I-Hyp/Hyp in DMSO/PEG400/water (25:60:15, v/v/v) or DMSO/saline (20:80, v/v) in the liver, spleen and lung were shown in Table I. Significantly higher values of radioactivity were found in the spleen and liver with ^{123}I-Hyp/Hyp in DMSO/saline (20:80, v/v) as compared to those with DMSO/PEG400/water (25:60:15, v/v/v) ($p<0.01$). The uptake in the spleen and liver was about 4.1-fold and 3-fold higher, respectively. Interestingly, radioactivity in lungs was comparable for both formulations.

Table I Distribution of Iodine-123-Labeled Hypericin/Hypericin (^{123}I-Hyp/Hyp) in Different Formulations in Organs of the Reticuloendothelial System (RES) Including the Liver, Lung and Spleen from Normal Rats ($N=6$/Formulation) at 24 h Post-injection

Organs	DMSO/saline		DMSO/PEG400/water		*p* (%ID/g)
	%ID ± SD	%ID/g ± SD	%ID ± SD	%ID/g ± SD	
Lungs	1.3 ± 0.5	1.1 ± 0.1	2.2 ± 1.2	1.5 ± 0.2	0.05
Liver	29.5 ± 0.8	2.6 ± 0.2	11.7 ± 4.1	0.9 ± 0.3	<0.01
Spleen	4.6 ± 0.1	6.3 ± 0.4	1.2 ± 0.7	1.4 ± 0.1	<0.01

%ID percentage of injected dose, *%ID/g* percentage of injected dose per gram, *SD* standard deviation, *DMSO* dimethyl sulfoxide, *PEG400* polyethylene glycol 400

Necrosis Avidity of ^{123}I-Hyp/Hyp

Table II shows the uptake of ^{123}I-Hyp/Hyp in DMSO/PEG400/water (25:60:15, v/v/v) or DMSO/saline (20:80, v/v) in necrotic and viable tissues from RPLI rats at 24 h post-injection.

By gamma counting, ^{123}I-Hyp/Hyp in DMSO/PEG400/water (25:60:15, v/v/v) showed a significantly higher accumulation in necrotic liver (4.6 ± 1.2%ID/g) and lower uptake (0.2 ± 0.1%ID/g) in viable liver ($p<0.01$), leading to necrosis-to-liver ratio of 21.8 ± 2.4. This was proven by autoradiography where radioactivity in dead areas higher than in normal liver was perfectly correlated to the corresponding H&E-stained slides (Fig. 5) with a necrotic-to-viable liver ratio as high as 26.2 ± 3.0 (Table II). On the other hand, very low tracer concentration in necrotic regions (0.4 ± 0.1%ID/g) and high radioactivity accumulation in viable liver (2.5 ± 0.02%ID/g) were found with ^{123}I-Hyp/Hyp in DMSO/saline (20:80, v/v) (Fig. 5), causing a dramatic drop of necrotic-to-viable liver ratios derived from gamma counting (0.2 ± 0.1) and autoradiography (1.0 ± 0.3).

Avidity of ^{131}I-Hyp/Hyp for Tumor Necrosis

By gamma counting, 1 day after injection of ^{131}I-Hyp/Hyp in DMSO/PEG400/water (25:60:15, v/v/v), mean uptake values were 1.7 ± 0.4%ID/g and 0.9 ± 0.1%ID/g in tumor necrosis and viable liver respectively, with a tumor-to-liver ratio of 1.9 ± 0.3.

Table II Necrosis Avidity of Iodine-123-Labeled Hypericin/Hypericin (^{123}I-Hyp/Hyp) in Different Formulations in Rats of Reperfused Partial Liver Infarction (RPLI) ($N=6$/Formulation) at 24 h Post-injection

Tissues	DMSO/saline		DMSO/PEG400/water	
	%ID ± SD	%ID/g ± SD	%ID ± SD	%ID/g ± SD
Necrotic liver	1.9 ± 0.9	0.4 ± 0.1	6.5 ± 1.9	4.6 ± 1.2
Liver	30.3 ± 0.1	2.5 ± 0.02	1.4 ± 0.6	0.2 ± 0.1
	p values (%ID/g)			
Necrotic liver *vs.* liver	<0.01		<0.01	
Liver	<0.01			
Necrotic liver	<0.01			
	Ratio (necrotic liver/liver)			
Gamma counting (%ID/g)	0.2 ± 0.1		21.8 ± 2.4	
Autoradiography DLU/mm^2	1.0 ± 0.3		26.2 ± 3.0	

%ID percentage of injected dose, *%ID/g* percentage of injected dose per gram, *DLU* digital light units, *SD* standard deviation, *DMSO* dimethyl sulfoxide, *PEG400* polyethylene glycol 400

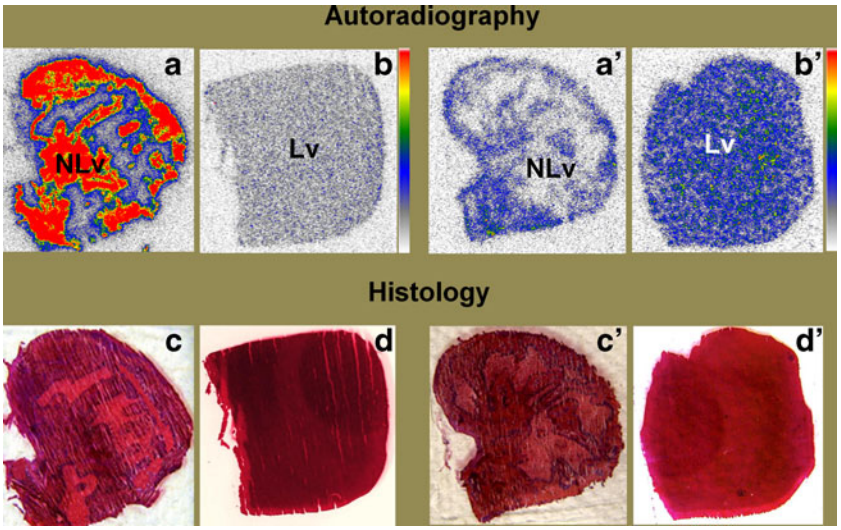

Fig. 5 Post-mortem analysis of necrotic and viable liver tissues from rats with reperfused partial liver infarction (RPLI) pre-injected with iodine-123-labeled-hypericin/hypericin (^{123}I-Hyp/Hyp) in different formulations. Autoradiograms from animals pre-injected with ^{123}I-Hyp/Hyp in DMSO/PEG400/water (25:60:15, v/v/v) revealed higher tracer uptake in necrotic areas (**a**) than in the viable liver (**b**), as confirmed by histology (**c**, **d**)*. The scattered low uptake areas in necrosis (**a**) referred to the "no-reflow" phenomenon in this animal model. Autoradiograms from animals receiving ^{123}I-Hyp/Hyp in DMSO/saline (20:80, v/v) showed less radioactivity accumulation in necrotic liver (**a'**) relative to its counterpart with different formulation (**a**), and higher tracer uptake in viable liver (**b'**) in comparison to (**b**)*. H&E-stained sections confirmed the presence of massive necrosis with scattered non-reperfused areas (**c'**) and the viable liver tissue (**d'**). * The colour code bar illustrates the coding scheme for the radioactivity. *Red colour* indicates regions with the highest ^{123}I-Hyp/Hyp activity while white encodes for the lowest radiotracer activity.

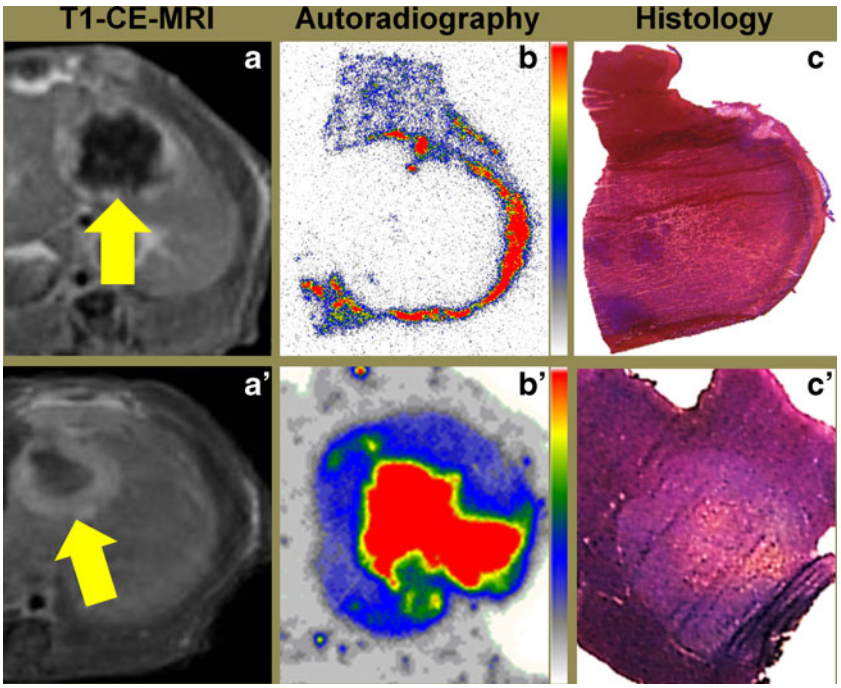

Fig. 6 T1-weighted contrast-enhanced magnetic resonance imaging (T1-CE-MRI), autoradiograms and histology co-localization in rats with implanted liver rhabdomyosarcoma (R1) having received ZD6126 to induce tumor necrosis followed 24 h later by ^{131}I-Hyp/Hyp in DMSO/PEG400/water (25:60:15, v/v/v) formulation. (**a**) One day after ^{131}I-Hyp/Hyp administration, T1-CE-MRI showed ZD6126-induced tumor devascularization and necrosis (*arrow*) accompanied with viable tumor residues as a thin rim enhancement with a non-enhanced core. (**b**) Autoradiogram of R1 liver tumor section showed a high radioactivity rim at the edge of the tumor necrosis*. (**c**) H&E stained section closely matched with the T1-CE-MRI and autoradiographic findings (**a**, **b**). (**a'**) Six days after ^{131}I-Hyp/Hyp injection, T1-CE-MRI showed no significant changes in tumor dimension with a thick hyperintense rim (*arrow*) suggesting the presence of viable tumor at the periphery. However, the tumor center remained hypointense indicating a lack of inward tumor re-growth due to most likely the tumoricidal effect of the centrally accumulated ^{131}I-Hyp/Hyp. (**b'**) Autoradiogram of R1 liver tumor section showed high radioactivity retention and moderate radioactivity in the peripheral viable tumor relative to the almost absent radioactivity in the surrounding liver*. (**c'**) The corresponding histological section proved the MRI and autoradiographic findings (**a'**, **b'**). * The *colour code bar* indicates the coding scheme for the ^{131}I-Hyp/Hyp radioactivity. *Red colour* represents regions with the highest radiotracer activity while *white* encodes for the lowest values.

By autoradiography, a characteristic rim of high radioactivity matched closely the peripheral edge of the tumor necrosis observed by CE-MRI and confirmed by H&E histology (Fig. 6). Radioactivity ratio between tumor necrosis and viable liver reached to 9.8 ± 1.7. This pattern shows the gradual entry and distribution of the radioiodinated hypericin into the tumor necrosis at early phase (24 h) after tracer injection (Fig. 6).

Tumoricidal Effects of ^{131}I- Hyp/Hyp

Table III illustrates the tumoricidal effects of the formulations of ^{131}I-Hyp/Hyp in R1 rats over 6 days post injection. No tumor necrosis could be discerned by CE-MRI before ZD6126 administration, whereas 24 h later, necrosis ratios were above 50% in all R1 tumors. On day 6 after ^{131}I-Hyp/Hyp treatment, the corresponding necrosis ratios were 40 ± 16% and 19 ± 11% ($p < 0.05$) for the formulation of DMSO/PEG400/water (25:60:15, v/v/v) and DMSO/saline (20:80, v/v), respectively.

For ^{131}I-Hyp/Hyp in DMSO/PEG400/water (25:60:15, v/v/v), a prominent tumoricidal effect was observed using CE-MRI. By gamma counting, high and persistent accumulation (3.1 ± 0.3%ID/g) of ^{131}I-Hyp/Hyp in tumor necrosis and low hepatic uptake (0.1 ± 0.01%ID/g) were detected. Rats treated with ^{131}I-Hyp/Hyp in DMSO/PEG400/water (25:60:15, v/v/v) had significantly ($p < 0.05$) smaller R1 tumor volumes (0.9 ± 0.3 cm^3) and slower tumor growth rate than the animals receiving ^{131}I-Hyp/Hyp in DMSO/saline (20:80, v/v) (Table III). On autoradiograms, a high amount of radioactivity appeared either partially or entirely in the tumor necrosis even several days after administration which confirm the long-term necrosis affinity of ^{131}I-Hyp/Hyp in a proper formulation (Fig. 6).

With ^{131}I-Hyp/Hyp in DMSO/saline (20:80, v/v), instead, no therapeutic effects were noted on day 6 post radioactivity injection. Quantitative tumor size measurement by CE-MRI showed rapid growth with an initial tumor volume of 0.4 ± 0.2 cm^3 contrasted with 2.6 ± 0.7 cm^3 ($p < 0.05$) at day 6 (Table III). By gamma counting, very low radioactivity in tumors (0.1 ± 0.04%ID/g) and high radioactivity in the liver (2.1 ± 0.7%ID/g) were found, as proven by autoradiography in correlation with histomorphology (Fig. 7), suggesting a massive endocytosis of the colloidal particles of ^{131}I-Hyp/Hyp in DMSO/saline (20:80, v/v) by the Kupffer cells rather than by the necrotic tissue in the tumor.

DISCUSSION

In systemic radiotherapy, an ideal targeting agent should localize at a high concentration preferentially on the disease site to deposit a sufficient cytotoxic radiation dose, whereas the circulating or non-targeted fraction should be rapidly cleared from normal organs to avoid treatment-related adverse effects (34,35). Unfortunately, such therapies often render normal tissues or organs under unnecessary radiation exposure during or after treatment, causing structural and/or functional damages. Therefore, it is crucial to identify and eliminate those factors that may hamper the utility and performance of a candidate radiotherapeutic agent.

Radioiodinated Hyp is a radiocompound of low molecular weight (<1 kDa) with striking and longstanding necrosis affinity, which makes it potentially useful for crossfire eradication of the tumor residues left especially after a necrosis-inducing treatment such as using a VDA. This is the essence underlying the dual targeting theragnostic approach of OncoCiDia (1,2).

However, in order to deliver sufficient amount of lethal radiation on cancer cells, it is crucial to elaborate a proper formulation of radioiodinated Hyp, which guarantees a high uptake and prolonged retention in tumor necrosis and

Table III Tumoricidal Effect of Iodine-131-Labeled Hypericin/Hypericin (^{131}I-Hyp/Hyp) in Different Formulations on Rats with Rhabdomyosarcomas Tumors ($N = 6$/Formulation) Over 6 Days After Radioactivity Administration

Formulation	Day 0		Day 6			
	TV ± SD (cm^3)	NR ± SD (%)	TV ± SD (cm^3)	NR ± SD (%)	%ID/g ± SD	
					Liver	Tumor
DMSO/saline (I)	0.4 ± 0.2	68 ± 14	2.6 ± 0.7	19 ± 11	2.1 ± 0.7	0.1 ± 0.04
DMSO/PEG400/water (II)	0.4 ± 0.2	71 ± 18	0.9 ± 0.3	40 ± 16	0.1 ± 0.01	3.1 ± 0.3
		p values				
TV-day 0 vs day 6		<0.05 (I)			<0.05 (II)	
NR-day 0 *vs.* day 6		<0.05 (I)			<0.05 (II)	
TV(I) *vs.* TV (II)		<0.05				

TV tumor volume, *NR* necrosis ratio, *%ID/g* percentage of injected dose per gram, *SD* standard deviation, *DMSO* dimethyl sulfoxide, *PEG400* polyethylene glycol 400

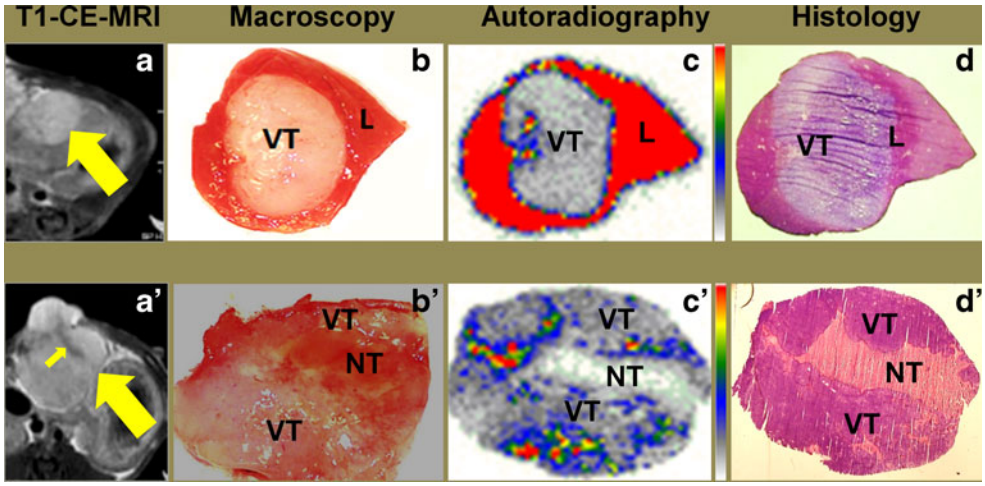

Fig. 7 T1-weighted contrast-enhanced magnetic resonance imaging (T1-CE-MRI), autoradiograms and histology co-localization 6 days after ^{131}I-Hyp/Hyp administration in rats with implanted liver rhabdomyosarcoma (R1) treated with ZD6126 and followed 24 h later by ^{131}I-Hyp/Hyp in DMSO/saline (20:80, v/v). Case one of complete tumor re-growth (**a-d**): (**a**) T1-CE-MRI showed a hyperenhanced R1 tumor (*arrow*) without an unenhanced necrotic core as shown in Fig. 6**a**, **a'**, suggesting inward tumor re-growth that replaced the ZD6126-induced central necrosis. (**b**) On the tissue section, the tumor looked viable (VT) clearly bordered with the surrounding normal liver (L). (**c**) On autoradiogram, a large amount of ^{131}I-Hyp/Hyp activity still retained in the normal liver (L) in comparison with the low tracer concentration in the emerging viable tumor (VT) tissue due to a lack of ^{131}I-Hyp/Hyp accumulation in the ZD6126-induced tumoral necrosis 6 days ago*. (**d**) H&E-stained specimen confirmed the MRI (**a**), macroscopic (**b**) and autoradiographic (**c**) findings. Case two of incomplete tumor re-growth (**a'-d'**): (**a'**) T1-CE-MRI showed a hyperenhanced, large solid mass (*arrow*) due to a lack of ^{131}I-Hyp/Hyp accumulation in ZD6126-induced central necrosis resulting in rapid repopulation of the residual cancer cells after administration of ^{131}I-Hyp/Hyp in DMSO/saline (20:80, v/v) formulation. Notice that a band of tumor (*small arrow*) was not enhanced suggesting the remaining tumor necrosis. (**b'**) On the tissue section, the tumor looked largely viable (VT) except a band of necrotic tumor (NT). (**c'**) On autoradiogram, no radioactivity accumulation was detected in necrotic tumor (NT)*. (**d'**) H&E stained section showed visible evidence of tumor necrosis (NT) and massive viable tumor (VT) and confirmed the MRI (**a'**), macroscopic (**b'**) and autoradiographic (**c'**) findings. * The *color code bar* represents the coding scheme for the ^{131}I-Hyp/Hyp radioactivity. *Red* and *white* colors encode regions with the highest and lowest radioactivity, respectively.

meanwhile a fast clearance from normal organs. Unfortunately, after the incorporation of an iodine atom into Hyp structure, ^{123}I-Hyp or ^{131}I-Hyp tends to aggravate the water insolubility that is a commonly confronted problem in the parenteral drug formulation. Consequently, it may form aggregates that lack necrosis avidity and retain largely in RES organs, leading to impaired safety and clinical efficacy. The current research was intended to investigate the impact of the formulations of radioiodinated Hyp under *in vivo* experimental conditions.

Based on previous experiments, we performed the radioiodination of Hyp by using Iodogen as oxidant. Since iodine is unreactive to benzene-based structures, it is treated with an oxidant to obtain electrophilic iodine which replaces an ortho proton on the aromatic ring of Hyp containing strongly activating substituent (-OH). It is a rapid, reproducible and simple method that specially offers good radiochemical yield for aromatic compounds like hypericin.

Since ^{123}I-Hyp and ^{131}I-Hyp share similar biological properties (36,37), the gamma-emitter iodine-123 with a half-life of 13.2 h was used for tests on tissue distribution and necrosis avidity. Because OncoCiDia has been intended as a dual-targeting anticancer radiotherapy, affinity for tumor necrosis and tumoricidal effects were assessed with ^{131}I-Hyp. Iodine-131 has a longer half-life (8.1 days) and emits beta-particles (maximal energy: 606 keV, tissue penetration of 0.6 to 2 mm) (38) that are able to destroy the nearby few layers of residual cancer cells left over after VDA treatment.

To address the tracer uptake in necrosis, we selected the study period at least 24 h after administration of ^{123}I-Hyp/Hyp or ^{131}I-Hyp/Hyp, which assured the bulky clearance of the circulating tracer from the healthy tissues and sufficient accumulation in necrotic regions. This also allowed distinguishing between aggregate retention in RES organs and early nonspecific distribution of the compound.

Both formulations for ^{123}I-Hyp/Hyp or ^{131}I-Hyp/Hyp were prepared using the cosolvent solubilization method, which is based on adding water-soluble solvents to an aqueous system to dissolve a water-insoluble solute. It has been one of the most common methods for delivering drugs (such as hypericin and its derivatives) (17) as a true solution in the smallest volume of liquid as possible. Although several theories have been put forward to account for cosolvency, the coexistence of both hydrophobic and hydrophilic groups in the solvent molecule can play a fundamental role. In fact, most of the cosolvents contain hydrogen bond donating/accepting groups and small hydrocarbon regions (e.g. PEG400). Their hydrogen bonding moieties guarantee the compound's miscibility with water whereas their hydrophobic chain interferes with hydrogen bond networks reducing the overall attraction

between water molecules (39). Other solvents lack of an acidic hydrogen but share ion dissolving power with protic solvents (e.g.: DMSO). As a consequence, the solubility of non-polar/hydrophobic compounds is increased through disrupting self-association of water molecules by the cosolvent. A different hypothesis states that cosolvents facilitate solute solubilization by making the solvent environment less polar, which promotes interactions between solute and solvent molecules (39). Nevertheless, further than these theories, it is a convenient method that allows minimizing the radiation exposure time during the radioactive drug formulation owing to its rapidness and simplicity.

As can be concluded from the biodistribution experiment in normal rats, when DMSO/PEG400/water (25:60:15, v/v/v) was used as vehicle, ^{123}I-Hyp/Hyp showed low uptake in RES organs. In contrast once it is dissolved in DMSO/saline (20:80, v/v), it was characterized by a high radioactivity accumulation in the spleen and liver. Most likely, before ^{123}I-Hyp/Hyp injection, the stacked association of Hyp occurs owing to the hydrophobic effect of its aromatic core molecules in the aqueous saline environment (26). Consequently, extensive aggregation of non-water soluble hypercinate salts arises in the formulation. These aggregates, once IV injected, are unlikely monomerized by serum proteins (e.g. low-density lipoprotein or LDL). Eventually, phagocytic cells of RES organs such as splenic cords and hepatic Kupfer cells dispose of these particles by engulfing, trapping and/or metabolizing them. Actually, this result confirms previous fluorescence spectroscopy and diffusion coefficient measurements performed by Bano *et al.*, in which Hyp remained in its monomeric form in DMSO/H_2O mixtures containing up to ~20–30 wt% water. However, at higher water concentration, it starts to disperse as colloidal non-fluorescent aggregates with high molecular weights (40). The size of such associates becomes larger with the increasing of the water concentration in the solvent mixture (38). Based on our results, it seems that Hyp and its radioiodinated derivatives (^{123}I-Hyp and ^{131}I-Hyp) exhibited similar biological behaviors. Indeed, the biodistribution of ^{123}I-Hyp/Hyp in DMSO/saline (20:80, v/v) is rather similar to the biodistribution pattern exhibited by certain colloidal radiopharmaceuticals that have been used for nuclear imaging of RES organs (41,42). Examples are ^{99m}Tc-sulfur colloid particles (0.1–1.0 μm) (41), ^{99m}Tc-Tin colloid (>0.5 nm) (43), *etc.*

The current findings are fully accordant with the previous studies performed using different formulations of unlabeled Hyp regarding the influence of the vehicle nature on its tissue distribution and biological activity (27). Despite the incorporation of iodine into Hyp structure, as was expected, both unlabeled Hyp and its iodinated derivative share rather similar solubility properties. Indeed, a similar trend was observed in the tissue-distribution of ^{123}I-Hyp/Hyp, either as aggregates or as true solution. For instance, with DMSO/saline (20:80, v/v) as vehicle, we noticed a maximum uptake in the spleen, followed by liver and lungs. Likewise, after injecting ^{123}I-Hyp/Hyp in DMSO/PEG400/water (25:60:15, v/v/v), lower accumulation was found in such organs with a relative high uptake in lungs and spleen followed by liver (27).

Concerning the necrosis avidity, similar patterns were observed with ^{123}I-Hyp/Hyp dissolved in different formulations on rats with RPLI. It seems the physical forms of the Hyp present in the delivery system influence substantially on its necrosis accumulation. By tissue gamma counting, a lack of necrosis avidity of ^{123}I-Hyp/Hyp aggregates in DMSO/saline (20:80, v/v) was reflected by low uptake values of 0.4%ID/g in necrotic liver with necrosis-to-viable tissues ratios as low as 0.2. On the other hand, with ^{123}I-Hyp/Hyp in DMSO/PEG400/water (25:60:15, v/v/v) as true solution, 4.6%ID/g was reached in hepatic necrosis leading to a ratio around 20. Another method used to characterize the necrosis affinity of ^{123}I-Hyp/Hyp was the calculation of the radioactivity ratio between dead and viable areas by quantitative (ROI)-based analysis of autoradiography on tissue sections. Because the difficulty of tissue sampling in a mixture of necrotic with viable tissue by means of tissue-gamma counting, a reduced necrotic-to-viable radioactivity ratio is often acquired. By using autoradiography, therefore, the ratio calculation can be corrected and become more accurate. Indeed, values over 25 and 1.0 are reached for radioiodinated hypericin in DMSO/PEG-400 (25:60:15, v/v/v) and DMSO/saline (20:80, v/v), respectively. In any case, however, the results from both methods verify the ability of DMSO and PEG400 and their combinations as cosolvents for Hyp or its derivatives.

The highly polar aprotic solvents (e.g.: DMSO) are able to dissolve monomolecular Hyp, enabling Hyp and derivatives as excellent necrosis avid agents. On the other hand, the peculiar structure of PEGs, specifically the hydrophobic hydrocarbon region reduces the dipole moment of water by breaking the hydrogen bonds between water molecules, which reduces overall intermolecular interactions and allows hydrophobic compounds such as Hyp or its iodinated derivatives to fit in (39). Evidently, to show necrosis avidity, radioactive Hyp should be present as a monomer, but not as an aggregate. Similarly, in the animal tumor model, the proper choice of a formulation, i.e. DMSO/PEG400/water (25:60:15, v/v/v), enabled radioiodinated Hyp to preserve its necrosis avidity that constitutes the cornerstone for the high tumor accumulation in implementation of OncoCiDia as a new targeted anticancer strategy.

In regard to the tumoricidal effects of ^{131}I-Hyp/Hyp, the delivery system plays a crucial role in the therapeutic outcome. Beyond the biological variability and differences in sensitivity of the exposed cells, the therapeutic success is determined by the ability of the targeting agent to deliver enough radiation on the surviving tumor cells and kill them.

Once ^{131}I-Hyp/Hyp is dissolved in a wrong formulation, insufficient lethal dose of radiation eventually is delivered on the tumor cells. Consequently, complete or partial tumor regression followed by rapid repopulation of viable cells remaining at the tumor periphery after VDA or appearance of new malignant lesions in close proximity to the primary site can occur. In contrast, when ^{131}I-Hyp/Hyp is in a proper formulation, it selectively inhabits the tumor necrosis at a high concentration and deposits lethal radiation to adjacent residual cancer cells for a prolonged period. The relative efficacy of systemic radiotherapy depends not only on the dose preferentially delivered into malignant tissue, as compared to normal tissue, but also on continuous irradiation deposit over a prolonged period from days to weeks, which appear both reachable with OncoCiDia if ^{131}I-Hyp/Hyp is properly formulated. As a consequence, improved cancer treatability or curability can be anticipated.

In conclusion, our study demonstrated that the formulation of radioidodinated Hyp can profoundly influence the biological behavior and therapeutic efficacy of the compound. The proper choice of the delivery system may help to prevent unwanted aggregation, distorted biodistribution and deprived necrosis avidity of radioidodinated Hyp.

ACKNOWLEDGMENTS AND DISCLOSURES

This study has been supported in part by the KU Leuven Molecular Small Animal Imaging Center MoSAIC (KUL EF/05/08) and the center of excellence *in vivo* molecular imaging research (IMIR); KU Leuven projects IOF-HB/08/009 and IOF-HB/12/018; the European Union (Asia-Link CfP 2006-EuropeAid/123738/C/ACT/Multi-Proposal No. 128-498/111), the National Natural Science Foundation of China (81071828), and Jiangsu Province Natural Science Foundation (BK2010594). The corresponding author is currently a Bayer Lecture Chair holder. The authors declare no conflict of interest.

REFERENCES

1. http://vimeo.com/44871398 Katholieke Universiteit Leuven – Oncocidia; Accessed on July 8, 2013.
2. Li J, Sun Z, Zhang J, Shao H, Cona MM, Wang H, *et al.* A dual-targeting anticancer approach: soil and seed principle. Radiology. 2011;260:799–807.
3. Friedl P, Wolf K. Tumour-cell invasion and migration: diversity and escape mechanisms. Nat Rev Cancer. 2003;3:362–74.
4. Hinnen P, Eskens F. Vascular disrupting agents in clinical development. Br J Cancer. 2007;96:1159–65.
5. Cona MM, Li J, Chen F, Feng Y, Alpizar YA, Vanstapel F *et al.* A safety study on single intravenous dose of tetrachloro-diphenyl glycoluril [iodogen] dissolved in dimethyl sulphoxide (DMSO). Xenobiotica. 2013. [Epub ahead of print].
6. Li JJ, Cona MM, Chen F, Feng Y, Zhou L, Zhang GZ *et al.* Sequential systemic administrations of Combretastatin A4 phosphate and radioiodinated hypericin exert synergistic targeted theranostic effects with prolonged survival on SCID mice carrying bifocal tumor xenografts. Theranostics. 2013;3(2):127–37.
7. Li J, Cona MM, Feng YB, Chen F, Zhang GZ, Fu XB, *et al.* A single-dose toxicity study in mice on non-radioactive iodinated hypericin for a targeted anticancer therapy. Acta Pharmacol Sin. 2012;33(12):1549–56.
8. Ni Y, Bormans G, Marchal G, Verbruggen A. Necrosis avid tracer agent. European Patent EP 1 651 201 B1, priority date: July 25, 2003.
9. Fonge HA, Bormans G, Ni Y, Chen F, Verbeke K, Marchal G, *et al.* Evaluation of mono-I-123- Hypericin as necrosis avid tracer agent. Eur J Nucl Med Mol Imaging. 2004;31(2):S381.
10. Sosa S, Pace R, Bornancin A, Morazzoni P, Riva A, Tubaro A, *et al.* Topical anti-inflammatory activity of extracts and compounds from Hypericum perforatum L. J Pharm Pharmacol. 2007;59:703–9.
11. Avato P, Raffo F, Guglielmi G, Vitali C, Rosato A. Extracts from St. John's wort and their antimicrobial activity. Phytother Res. 2004;18(3):230–2.
12. Sun ZP, Ni Y. Iodogen method for preparation of hypericin radioactive iodine marker Patent CN 200910013998.8; Publish date: July 8, 2009.
13. Bormans G, Huyghe D, Christiaen A, Verbeke K, de Groot T, Vanbilloen H, *et al.* Preparation, analysis and biodistribution in mice of iodine-123 labelled derivatives of hypericin. J Label Compd Radiopharm. 2004;47:191–8.
14. Hermanson GT. Bioconjugate techniques (Second Edition). In: Academic Press; 2008. p 554. ISBN: 978-0-12-370501-3.
15. Santa Cruz and Biotechnology. 2013 January 4. Available from: http://www.scbt.com/datasheet-3530-hypericin.html.
16. Miccoli L, Beurdeley-Thomas A, De Pinieux G, Sureau F, Oudard S, Dutrillaux B. Light-induced photoactivation of hypericin affects the energy metabolism of human glioma cells by inhibiting hexokinase bound to mitochondria. Cancer Res. 1998;58:5777–86.
17. Head CS, Luu Q, Sercarz J, Saxton R. Photodynamic therapy and tumor imaging of hypericin-treated squamous cell carcinoma. World J Surg Oncol. 2006;4:87.
18. Chung PS, Rhee CK, Kim KH, Paek W, Chung J, Paiva MB, *et al.* Intratumoral hypericin and KTP laser therapy for transplanted squamous cell carcinoma. Laryngoscope. 2000;110:1312–6.
19. Assadi A, Zarrindast MR, Jouyban A, Samini M. Comparing of the effects of hypericin and synthetic antidepressants on the expression of morphine-induced conditioned place preference. Iran J Pharm Res. 2011;10(3):619–26.
20. Kamuhabwa AA, Cosserat-Gerardin I, Didelon J, Notter D, Guillemin F, Roskams T, *et al.* Biodistribution of hypericin in orthotopic transitional cell carcinoma bladder tumors: implication for whole bladder wall photodynamic therapy. Int J Cancer. 2002;97:253–60.
21. Huygens A, Kamuhabwa AR, de Witte PAM. Stability of different formulations and ion pairs of Hypericin. Eur J Pharm Biopharm. 2005;59:461–8.
22. Miskovsky P. Hypericin – a new antiviral and antitumor photosensitizer: mechanism of action and interaction with biological macromolecules. Curr Drug Targets. 2002;3:55–84.
23. Falk H, Meyer J. On the homo- and heteroassociation of hypericin. Monatsh Chemie. 1994;125:753–62.
24. Yamazaki T, Ohta N, Yamazaki I, Song PS. Excited-state properties of hypericin: electronic spectra and fluorescence decay kinetics. J Phys Chem. 1993;97:7870–5.
25. Weiner L and Mazur Y. EPR studies of hypericin: photogeneration of free radicals and superoxide. J Chem Soc Perkin Trans. 1992;1439–1442.
26. Lavie G, Mazur Y, Lavie D, Meruelo D. The chemical and biological properties of hypericin: a compound with a broad spectrum of biological activities. Med Res Rev. 1995;15:111–9.

27. Van de Putte M, Roskams T, Bormans G, Verbruggen A, de Witte P. The impact of aggregation on the biodistribution of hypericin. Int J Oncol. 2006;28:655–60.
28. Ghaedi M, Montazerozohori M, Behfar M, Marahel F. Influence of multiwalled carbon nanotubes on the response performance of carbon paste iodide ion selective electrode based on iron (II) phthalocyanine. Int J Electrochem Sci. 2011;6:6074–84.
29. Sihvera W, Biera D, Holschbach MH, Schulze A, Wutz W, Olsson RA, *et al.* Binding of tritiated and radioiodinated ZM241,385 to brain A2A adenosine receptors. Nucl Med Biol. 2004;31:173–7.
30. Fonge H, Van de Putte M, Huyghe D, Bormans G, Ni Y, de Witte P, *et al.* Evaluation of tumor affinity of mono-[^{123}I]iodohypericin and mono-[^{123}I]iodoprotohypericin in a mouse model with a RIF-1 tumor. Contrast Media Mol Imaging. 2007;2:113–9.
31. Ni Y, Huyghe D, Verbeke K, de Witte PA, Nuyts J, Mortelmans L, *et al.* First preclinical evaluation of mono-[^{123}I]iodohypericin as a necrosis-avid tracer agent. Eur J Nucl Med Mol Imaging. 2006;1:1–7.
32. Wu X, Wang H, Chen F, Jin L, Li J, Feng Y, *et al.* Rat model of reperfused partial liver infarction: characterization with multiparametric magnetic resonance imaging, microangiography, and histomorphology. Acta Radiol. 2009;50:276–87.
33. Chen F, Sun X, De Keyzer F, Yu J, Peeters R, Coudyzer W, *et al.* Liver tumor model with implanted rhabdomyosarcoma in rats: MR imaging, microangiography, and histopathologic analysis. Radiology. 2006;239:554–62.
34. Volkert WA, Hoffman TJ. Therapeutic radiopharmaceuticals. Chem Rev. 1999;99:2269–92.
35. Liu S, Edwards DS. Bifunctional chelators fortherapeutic lanthanide radiofarmaceuticals. Bioconjug Chem. 2001;12:7–34.
36. Van de Putte M, Marysael T, Fonge H, Roskams T, Cona MM, Li J, *et al.* Radiolabeled iodohypericin as tumor necrosis avid tracer: diagnostic and therapeutic potential. Int J Cancer. 2012;131(2):E129–37.
37. Li J, Cona MM, Chen F, Feng Y, Zhou L, Yu J, *et al.* Exploring theranostic potentials of radioiodinated hypericin in rodent necrosis models. Theranostics. 2012;2(10):1010–9.
38. Skugor M. Thyroid disorders. A Cleveland clinic guide. Cleveland Clinic Press; 2006. p. 82. ISBN 978-1-59624-021-6.
39. Millard JW, Alvarez-Núñez FA, Yalkowsky SH. Solubilization by cosolvents establishing useful constants for the log-linear model. Int J Pharm. 2002;245:153–66.
40. Bánó G, Staničová J, Jancura D, Marek J, Bánó M, Uličný J, *et al.* On the diffusion of hypericin in dimethylsulfoxide/water mixtures-the effect of aggregation. J Phys Chem B. 2011;115:2417–23.
41. Vallabhajosula S, Killeen RP, Osborne JR. Altered biodistribution of radiopharmaceuticals: role of radiochemical/pharmaceutical purity, physiological, and pharmacologic factors. Semin Nucl Med. 2010;40:220–41.
42. Tsopelas C, Smith E, Drew PA, Bartholomeusz FDL. Preparation and biological evaluation of [^{99m}Tc]stannous fluoride colloid-labelled-leucocytes in rats [^{99m}Tc]stannous fluoride labelled-leucocytes in rats. J Label Compd Radiopharm. 2003;46:751–63.
43. Imoto S, Murakami K, Ikeda H, Fukukita H, Moriyama N. Mammary lymphoscintigraphy with various radiopharmaceuticals in breast cancer. Ann Nucl Med. 1999;13:325–9.